MNRAS 000, 1–16 (2024) Preprint 18 December 2024 Compiled using MNRAS LaTeX style file v3.3

BSN: The First In-Depth Photometric Study of Seven Total Eclipse Contact Binary Systems

A. Poro,[1,2]★ K. Li,[3] E. Paki,[4] S. Baudart,[5] R. Michel,[6]† D. Valls-Gabaud,[1] L. Wang,[3] E. Fernández Lajús,[7] F. Alicavus[8.9] S. Foschino,[10] H. Aceves,[6] and F.J. Tamayo,[11]
[1] *LUX, Observatoire de Paris, CNRS, PSL, 61 Avenue de l'Observatoire, 75014 Paris, France*
[2] *Astronomy Department of the Raderon AI Lab., BC., Burnaby, Canada*
[3] *School of Space Science and Physics, Institute of Space Sciences, Shandong University, Weihai, Shandong 264209, People's Republic of China*
[4] *BSN Project; independent researcher, Tehran, Iran*
[5] *Commission des étoiles doubles, Société Astronomique de France, Paris, France*
[6] *Instituto de Astronomía, UNAM. A.P. 106, 22800 Ensenada, BC, México*
[7] *Instituto de Astrofísica de La Plata (CCT La Plata-CONICET-UNLP), La Plata, Argentina*
[8] *Çanakkale Onsekiz Mart University, Faculty of Arts and Sciences, Department of Physics, 17020, Çanakkale, Türkiye*
[9] *Çanakkale Onsekiz Mart University, Astrophysics Research Center and Ulupnar Observatory, 17020, Çanakkale, Türkiye*
[10] *Observatoire des Baronnies Provençales, LABSCAN, 1480 Route des Alpes, 05150 Moydans, France*
[11] *Facultad de Ciencias Físico-Matemáticas, UANL, 66451 San Nicolás de los Garza, NL, México*

Accepted XXX. Received YYY; in original form ZZZ

ABSTRACT

This is the first in-depth study of seven total eclipse W Ursae Majoris (W UMa)-type contact binary systems using photometric light curves. The ground-based observations were conducted with four observatories in the northern and southern hemispheres. We also used the Transiting Exoplanet Survey Satellite (TESS) for four target systems. We presented the analysis of orbital period variations of six systems and found that they display parabolic variations. The material transfer rates between the stars of the systems were calculated. Also, the results show that four systems have a long-term increase, while two of them have a long-term decrease in their orbital periods. We performed a light curve analysis using the PHysics Of Eclipsing BinariEs (PHOEBE) Python code and the Markov Chain Monte Carlo (MCMC) algorithm. Six of the target systems required the addition of a cold or hot starspot. We estimated absolute parameters using the $P-a$ empirical relationship. According to each component's effective temperature and mass, it was recognized that the studied systems are W-subtype. We examined the dynamic stability of two targets, which were low mass ratio contact binary systems. We also showed the evolution of stars in the $M-R$ and $M-L$ diagrams. Finally, we showed that the hotter stars in contact systems have a temperature difference of less than ≈ 400 K compared to the Gaia DR3 temperature report.

Key words: Contact binary stars - Fundamental parameters of stars - Astronomy data analysis - Individual (Seven Contact Binary Stars)

1 INTRODUCTION

Among the extremely wide variety of binary stars, overcontact systems that exchange mass, angular momentum, and energy are important to assess the physical mechanisms at play, such as coalescence, spiraling, angular momentum loss, thermal relaxation oscillations, etc (Lucy 1968, Bradstreet et al. 1994, Eggleton & Kiseleva-Eggleton 2002, Qian 2003, Yakut & Eggleton 2005, Stepien 2006, Stepien 2011, Eggleton 2012). W UMa-type contact binaries have two main-sequence components of F to K spectral type, short (< day) periods, and a common convective envelope. The W UMa-type binaries are challenging to study. The minimum depths of primary and secondary eclipses are similar, and the effective temperatures of the components are also close to each other (Kuiper 1941, Qian et al. 2014). Morphologically, their light curves are classified into two types: in the A-subtype, the more massive component has a higher effective temperature, while in the second class, the W-subtype, the reverse is true (Binnendijk 1970). W-subtype systems also have shorter periods, later spectral types, and larger mass ratios. Some systems have transitioned from the A-subtype to the W-subtype in a few years (Latković et al. 2021).

The broadening and blending of spectral lines make it difficult to measure some contact systems' mass ratios (q) spectroscopically, and hence the best estimates come from the photometric analysis of systems undergoing total eclipses. Also, estimating the mass ratio for systems where one of the companions has a small radius and mass is difficult and sometimes not possible with spectroscopic data, and photometric analysis is an effective way to study them (Li et al. 2022, Li et al. 2024a).

★ E-mail: atilaporo@bsnp.info
† E-mail: rmm@astro.unam.mx

Many studies have been done about the orbital period of contact binary systems and its relationship with other physical parameters. So, the accurate determination of the orbital period can have an impact on other empirical parameter relationships to estimate the absolute parameters (Qian 2003).

One of the most prevalent features of contact binary systems is the well-known O'Connell effect (O'Connell 1951a). The asymmetry in the light curve maxima of eclipsing binary stars is indicative of this effect. This phenomenon, which leads to the need to include the star spot(s) in the light curve solution, can be explained by the presence of magnetic activity at the star's surface.

This study used photometric observations of the seven W UMa-type contact binaries undergoing total eclipses at four observatories to provide more accurate orbital and physical parameters. The paper is divided into seven sections. The study is divided into seven sections. Section 2 recaps the basic known properties of the selected systems, while Section 3 reports the observations carried out at the different ground-based observatories and the TESS mission. Section 4 analyzes orbital period variations of the systems while Section 5 presents the multi-color light curve solutions. Absolute parameter estimations are discussed in Section 6. Section 7 discussed and summarized our results.

2 TARGET SYSTEMS

We have analyzed seven eclipsing binary stars, including BK Oct, Gaia DR3 5842836641483889280 (hereinafter G5842), ASAS J165337+1542.7 (hereinafter J1653), CRTS J165528.6+294254 (hereinafter J1655), NSVS 5902490 (hereinafter N5902), NSVS 5905978 (hereinafter N5905), and V2825 Ori. The following are the target systems' introductions:

• BK Oct: Hoffmeister (1963) and Kukarkin et al. (1970) reported this system as a new variable from the southern hemisphere. Then, Malkov et al. (2006) and Avvakumova et al. (2013) are classified BK Octans as a contact binary star. The General Catalogue of Variable Stars (GCVS) reported 14.30 mag. as a maximum magnitude. The reported orbital periods of this system in the catalog are very close to each other: GCVS=0.3686 days, the Zwicky Transient Facility (ZTF)=0.3685127 days, the All-Sky Automated Survey for Supernovae (ASAS-SN)=0.36851 days, and the Wide-field Infrared Survey Explorer (WISE) catalog of periodic variable stars=0.3685174 days. It should be mentioned that the temperature difference reported from Gaia Data Release 3 (DR3) and TESS Input Catalog (TIC) v8.2 with 6023 ± 177 K is significant for this system.

• G5842: This system was proposed for the first time in the study of Mowlavi et al. (2023) as a contact binary candidate. It is not listed in catalogs such as ASAS-SN and GCVS, and there is little information about it. Also, G5842 has not been observed by TESS yet.

• J1653: It is located in the Hercules constellation in the northern hemisphere. J1653 was discovered by the Robotic Optical Transient Search Experiment I (ROTSE-I) telescope, which presented the first results of a search for periodic variable stars (Akerlof et al. 2000). The ZTF periodic variable stars catalog presented an ephemeris for this system as $2458638.293583^{HJD} + 0.2809766 \times E$ (Chen et al. 2020). The ASAS and Variable Star Index (VSX) catalogs reported 13.20 mag. and 13.16 mag. for the maximum magnitude of this binary system. TIC reported a system temperature of 5337 ± 154, which is 226 K higher than Gaia DR3.

• J1655: This binary system was discovered by Catalina Surveys Data Release-1 (CSDR1; Drake et al. 2014) in the constellation Hercules. The CSDR1, VSX, ZTF, and ASAS-SN catalogs reported J1655 as a contact system with an orbital period of 0.26999 days. The VSX database reported 16.40 mag. for the maximum magnitude of this binary system. Also, the temperature difference between Gaia DR3 and TIC is only 80 K for this system (T_{TIC} = 4737 ± 165).

• N5902: It was discovered as a W UMa binary binary system in the Northern Sky Variability Survey (NSVS; Hoffman et al. 2009). It is classified in the ASAS-SN, ZTF, and Asteroid Terrestrial-impact Last Alert System (ATLAS) catalogs as a contact binary system. N5902 is located in the Cygnus constellation, and its maximum magnitude was reported at 12.67 mag. by the VSX database. The temperature of this system is not reported in TIC.

• N5905: This binary system was discovered in the NSVS as a W UMa with an orbital period of 0.43319 days. N5905 is in the Cygnus constellation, and the VSX database presented V_{max} = 13.623 magnitude. The most important thing about this system is the huge temperature difference (911 K) reported by Gaia DR3 and TIC. As listed in Table 1, Gaia DR3's temperature is 5562 K and TIC reported 6473(278) K.

• V2825 Ori: Diethelm (2011) presented an ephemeris ($2454519.566^{HJD} + 0.346327 \times E$) for this binary system for the first time. V2825 Orion was classified as a contact binary by Kazarovets et al. (2015). Also, catalogs such as ATLAS, GCVS, and ASAS-SN introduced it as a contact binary system. GCVS and ASAS-SN have reported orbital period values of 0.346327 and 0.34633, respectively, which are close to each other. The ASAS Catalog of Variable Stars and GCVS catalogs reported 12.71 mag. and 12.75 mag. for maximum magnitudes, respectively. Regarding the system temperature, TIC reported a temperature that was 101 K higher than Gaia DR3 with a 315 K uncertainty.

3 OBSERVATION AND DATA REDUCTION

Photometric observations and data reductions were conducted for seven target systems using standard filters at four Northern and Southern Hemispheres observatories: Complejo Astronomico El Leoncito (CASLEO), San Pedro Martir (SPM), Observatoire Astronomique de Sabichette (OASa), and Deep Sky Chile.

3.1 CASLEO Observatory

The 2.15-meter Jorge Sahade (JS) telescope at the CASLEO Observatory in Argentina (69°18′ West, 31°48′ South, 2552 m above sea level) was used to observe the BK Oct. The standard BVR_cI_c filters and a CCD Versarray 2048B (Roper Scientific, Princeton Instruments) were employed. Moreover, binning 5 × 5 and a scale of 0.15 asec/pix were used for the observations. CCD reduction and aperture photometry were performed using the Image Reduction and Analysis Facility (IRAF[1]) APPHOT photometry program (Tody 1986). Bias and flat-field images were used in these data reduction processes.

3.2 SPM Observatory

The J1655 and J1653 binary systems were observed at the SPM Observatory in Mexico (115° 27' 49" West, 31° 02' 39" North, and an altitude of 2830 m above sea level). A 0.84-meter Ritchey-Chretien telescope (f/15), a CCD detector from Spectral Instruments (e2v CCD42-40 chip with $13.5 \times 13.5\mu 2$ pixels, gain of $1.39e-/$ ADU, and readout noise of $3.54e-$) and BVR_cI_c filters were used

[1] http://iraf.noao.edui

Table 1. Specifications of the target systems from the Gaia DR3.

System	RA.°(J2000)	Dec.°(J2000)	d(pc)	T_{Gaia}(K)
BK Oct	295.7660936	-74.8582357	1040(16)	5722
Gaia DR3 5842836641483889280 (G5842)	186.5547148	-71.2480380	1003(34)	4869
ASAS J165337+1542.7 (J1653)	253.4041846	15.7104837	434(6)	5111
CRTS J165528.6+294254 (J1655)	253.8694590	29.7150252	938(23)	4817
NSVS 5902490 (N5902)	320.4745956	39.5369870	621(34)	5722
NSVS 5905978 (N5905)	321.2055036	40.1329269	696(6)	5562
V2825 Ori	93.6080081	-0.5280932	531(5)	5920

for the observations. Photometric images were processed using IRAF routines (Tody 1986). The data reduction process was done using bias and flat-field images.

3.3 OASa Observatory

We have observed the N5902, N5905, and V2825 Ori systems at the OASa observatory in Toulon, France (05° 54' 35" East, latitude 43° 8' 59" North, and altitude 68 meters above sea level). We employed an apochromatic refractor telescope with a 102mm aperture, a ZWO ASI 1600MM CCD, and a V standard filter for observations of these binary systems. During the observations, the CCD average temperature was $-15°C$, and the image binning was set to 1×1. We performed the data reduction process using the Siril software 1.2.0[2], employing bias, dark, and flat-field images.

3.4 Deep Sky Chile Observatory

The G5842 target system was observed at the Deep Sky Chile Observatory, MPC code X07 (−30° 31' 35" South, −70° 51' 13.00" West, and altitude 1700 meters above sea level). We used a RASA 14-inch (f/2.2) telescope, ASI ZWO 6200 MM pro (CMOS) CCD, and a R_c standard filter. During observations, the CCD average temperature was $-15°C$, and the image binning set 1×1. The data reduction processes were carried out using C-Munipack 2.1.32 software[3] and the bias, dark, and flat-field images.

3.5 TESS Observations

NASA launched the TESS intending to discover exoplanets (Ricker et al. 2010, Ricker et al. 2015a. However, this telescope gave researchers high-precision photometric data from binary systems (Stassun et al. 2018). This space telescope has four wide-field cameras that allow it to observe different sky regions. TESS spends 27.4 days per sector observing a specific area of the sky. We used time-series available TESS data for the J1655, N5902, N5905, and V2825 Ori target systems. TESS data is available at the Mikulski Space Telescope Archive (MAST)[4]. TESS-style curves were extracted from the MAST using the LightKurve[5] code. The data was detrended using the TESS Science Processing Operations Centre (SPOC) pipeline (Jenkins et al. 2016). Table 4 lists the TESS sectors used in this study.

4 ORBITAL PERIOD VARIATIONS

In order to conduct further analysis on these targets, we strive to gather as many eclipsing times as we can from diverse photometric surveys, including the All-Sky Automated Survey for SuperNovae (ASAS-SN; Shappee et al. 2014; Jayasinghe et al. 2018), the Zwicky Transient Facility (ZTF; Bellm et al. 2019; Masci et al. 2019), the Transiting Exoplanet Survey Satellite (TESS; Ricker et al. 2015b) and Wide Angle Search for Planets (SuperWASP; Butters et al. 2010). Through these eclipsing times, we analyzed the orbital period variations for these seven targets. However, due to an insufficient number of eclipsing times collected for G5842, further analysis could not be conducted. In addition, we also collected data from O-C Gateway. We calculated directly the eclipsing times for TESS 2-min, TESS 10-min, and SuperWASP data. However, for the TESS 30-min cadence data, ZTF, and ASAS-SN dispersed data, we need to apply the method suggested by Li et al. (2020) to shift the data into one period before obtaining the eclipsing times. After that, we use the Kwee & van Woerden (1956) method to calculate the eclipsing times.

Since our data contains both the Barycentric Julian Date in Barycentric Dynamical Time (BJD_{TDB}) and the Heliocentric Julian Date (HJD), to unify the time scale, we used the online tool[6] to convert HJD to BJD_{TDB}. The eclipsing times extracted from our observations are listed in Table 5. The online machine-readable format is available for the extracted and collected minima times of the BK Oct, J1653, J1655, N5902, N5905, and V2825 Ori binary systems. Then, we calculated the O-C values using the reference ephemeris,

$$BJD = BJD_0 + P \times E, \tag{1}$$

where BJD is the observational eclipsing times, BJD_0 listed in the second column of Table 6 is the initial primary eclipsing time, and P listed in the third column of Table 6 is the orbital period. The calculated O-C values are displayed in Table 5 and the online machine-readable format, and the O-C diagrams are shown in Figure 1.

We find that all targets display parabolic variations; hence, we utilize the following equation for the O-C fitting,

$$O - C = \Delta T_0 + \Delta P_0 \times E + \frac{\beta}{2} E^2. \tag{2}$$

[2] https://siril.org/fr/download/2023-09-15-siril-1.2.0/
[3] https://c-munipack.sourceforge.net/
[4] https://mast.stsci.edu/portal/Mashup/Clients/Mast/Portal.htmL
[5] https://lightkurve.github.io/lightkurve/
[6] https://astroutils.astronomy.osu.edu/time/hjd2bjd.html

Table 2. Specifications of the ground-based observations.

System	Observation(s) Date	Filter	Exposure time(s)	Observatory
BK Oct	2024 (Aug. 9)	BVR_cI_c	$B(40)$, $V(15)$, $R_c(10)$, $I_c(10)$	CASLEO
G5842	2023 (March 2)	R_c	$R_c(120)$	Deep Sky Chile
J1653	2024 (May 27)	BVR_cI_c	$B(70)$, $V(50)$, $R_c(35)$, $I_c(30)$	SPM
J1655	2024 (May 21, June 1)	BVR_cI_c	$B(70)$, $V(50)$, $R_c(35)$, $I_c(30)$	SPM
N5902	2023 (July 2,9,14)	V	$V(110)$	OASa
N5905	2023 (July 2,9,14)	V	$V(110)$	OASa
V2825 Ori	2024 (March 1,6,18)	V	$V(110)$	OASa

Table 3. List the comparisons and check stars in the ground-based observations. Coordinates come from the Gaia DR3.

System	Star Type	Star Name	RA.°(J2000)	DEC.°(J2000)
BK Oct	Comparison	2MASS 19421402-7453083	295.5584457	-74.8856418
BK Oct	Check	2MASS 19425752-7455468	295.7397603	-74.9297148
G5842	Comparison	Gaia DR3 5842837401701627520	186.5597689	-71.2396145
G5842	Check	Gaia DR3 5842837264262660608	186.4736675	-71.2588317
J1653	Comparison	Gaia DR3 4557874824155774848	253.3489128	15.6819645
N1072	Check	Gaia DR3 4557880596591908352	253.4570287	15.7443665
J1655	Comparison	Gaia DR3 1309731726953037056	253.9057075	29.7599072
J1655	Check	Gaia DR3 1309729562289519488	253.8264715	29.6808101
N5902	Comparison	Gaia DR2 1965471833170939904	321.0915760	39.9935854
N5902	Check	Gaia DR2 1965424588530688256	321.0945478	39.9242306
N5905	Comparison	Gaia DR2 1965424588530688256	321.0945478	39.9242306
N5905	Check	Gaia DR2 1965424588530688256	321.0945478	39.9242306
V2825 Ori	Comparison	Gaia DR2 3121651740485309312	93.6216639	-0.5466014
V2825 Ori	Check	Gaia DR2 3121187540419633792	94.0583165	-1.0955787

Table 4. Specifications of the TESS data used in this investigation.

System	TIC	TESS Sector	Exposure time(s)	Obs. Year
J1653	353179421	25	1800	2020
N5902	373662724	15-16-55-56-75	1800-1800-600-200-200	2020-2021-2023-2-23-2024
N5905	468470819	15-16-55-56-75	1800-1800-600-200-200	2020-2021-2023-2-23-2024
V2825 Ori	242128030	6-33	1800-600	2018-2020

The fitted parameters are shown in Table 7, and the corrected new ephemeris is shown in Table 6. We found four stars show a long-term increase in their orbital periods, while two stars show a long-term decrease.

5 LIGHT CURVE SOLUTIONS

The light curve of the target binary systems was examined using the PHOEBE Python code version 2.4.9 and MCMC approach (Prša et al. 2016, Conroy et al. 2020). We used new ephemeris (Table 6) to convert time to phase in light curves. The contact mode was chosen for the light curve solutions based on the light curves' appearance, the systems' type in catalogs, and the short orbital periods. We assumed that $g_1 = g_2 = 0.32$ (Lucy 1967) and $A_1 = A_2 = 0.5$ (Ruciński 1969) were the gravity-darkening coefficients and the bolometric albedo, respectively. The Castelli & Kurucz (2004) study was used to model the stellar atmosphere, and the limb darkening coefficients were included as a free parameter in PHOEBE.

To begin the analysis, we used the Gaia DR3 database to find the input effective temperature. We also checked the temperature that the TESS input catalog v8.2 provided during the analysis process. The systems' initial temperatures were placed on the hotter star based on the depth of the minima. So, we used the difference in depth between the primary and secondary minima of the light curves to determine the temperature of the cooler component.

We estimated the systems' initial mass ratio using the q-search method (Terrell & Wilson 2005). We searched a range of mass ratios between $q = 0.1$ and $q = 10$. Then, we shortened the interval and searched again according to the minimum sum of squared residuals.

Table 5. The times of minima extracted from our observations.

System	Min.(BJD_{TDB})	Error	Epoch	O-C
BK Oct	2460532.52764	0.03099	0	0
	2460532.71410	0.03527	0.5	0.00220
G5842	2460005.69208	0.00027		
	2460005.82596	0.00021		
J1653	2460457.67965	0.00035	-0.5	0.00155
	2460457.81859	0.00072	0	0
	2460457.96061	0.00035	0.5	0.00153
J1655	2460451.72475	0.00054	-41	-0.00070
	2460462.79512	0.00029	0	0
	2460462.92888	0.00026	0.5	-0.00124
N5902	2460128.45307	0.00030	-20	0.00072
	2460135.47589	0.00103	0	0
	2460139.51393	0.00030	11.5	-0.00049
N5905	2460128.52808	0.00077	0	0
	2460135.45701	0.00100	16	-0.00199
	2460139.57193	0.00029	25.5	-0.00231
V2825 Ori	2460376.36072	0.00035	0	0
	2460388.31173	0.00024	34.5	0.00262

Table 6. Reference and new ephemeris of the systems. The referent times of minima (t_0) were obtained from our observations in this study.

System	Reference ephemeris		New ephemeris	
	t_0	Period/Source	Corrected t_0	New Period
BK Oct	2460532.5276(310)	0.3685127/ASAS-SN	2460532.5287(25)	0.3685138(16)
J1653	2460457.8186(7)	0.2809786/ASAS-SN	2460457.8205(24)	0.2809771(16)
J1655	2460462.7951(3)	0.2699918/ASAS-SN	2460462.7951(25)	0.2699975(10)
N5902	2460135.4759(10)	0.3511768/ASAS-SN	2460135.4758(1)	0.3511794(1)
N5905	2460128.5281(8)	0.4331826/VSX	2460128.5266(1)	0.4331824(2)
V2825 Ori	2460376.3607(4)	0.3463300/ASAS-SN	2460376.3629(5)	0.3463328(1)

Table 7. The O-C fitting coefficients and mass transfer rate.

Parameter	ΔT_0 ($\times10^{-4}d$)	Error	ΔP_0 ($\times10^{-7}d$)	Error	β ($\times10^{-7}d\ yr^{-1}$)	Error	dM_1/dt ($\times10^{-7}M_\odot\ yr^{-1}$)	Error
BK Oct	11.00	25.15	11.36	15.71	-4.93	3.62	1.29	0.95
J1653	18.71	24.38	-15.44	15.69	6.73	5.81	-2.67	2.3
J1655	-0.56	24.53	56.54	9.79	4.56	2.02	-3.1	1.37
N5902	-1.00	1.36	26.00	1.36	1.87	0.17	-0.79	0.07
N5905	-15.04	1.49	-1.76	1.83	-1.33	0.24	-0.30	0.05
V2825 Ori	21.57	4.57	28.40	1.47	3.22	0.14	-2.86	0.12

Figure 2 illustrates that each q-search curve has a clear minimum sum of squared residuals. Also, the mass ratio of total systems in photometric data is more reliable based on theory and empirical studies (Li et al. 2021, Sarvari et al. 2024).

The maxima of the light curves (phases 0.25 and 0.75) show asymmetry in the light curve for six target systems. The most probable explanation is that the magnetic activity of the components is causing the presence of the starspot(s), which are introduced with the O'Connell effect (O'Connell 1951b, Sriram et al. 2017). So, the light curve solution required a starspot on a component. Table 8 lists a starspot's commonly recognized features, including colatitude, longitude, angular radius, and temperature ratio.

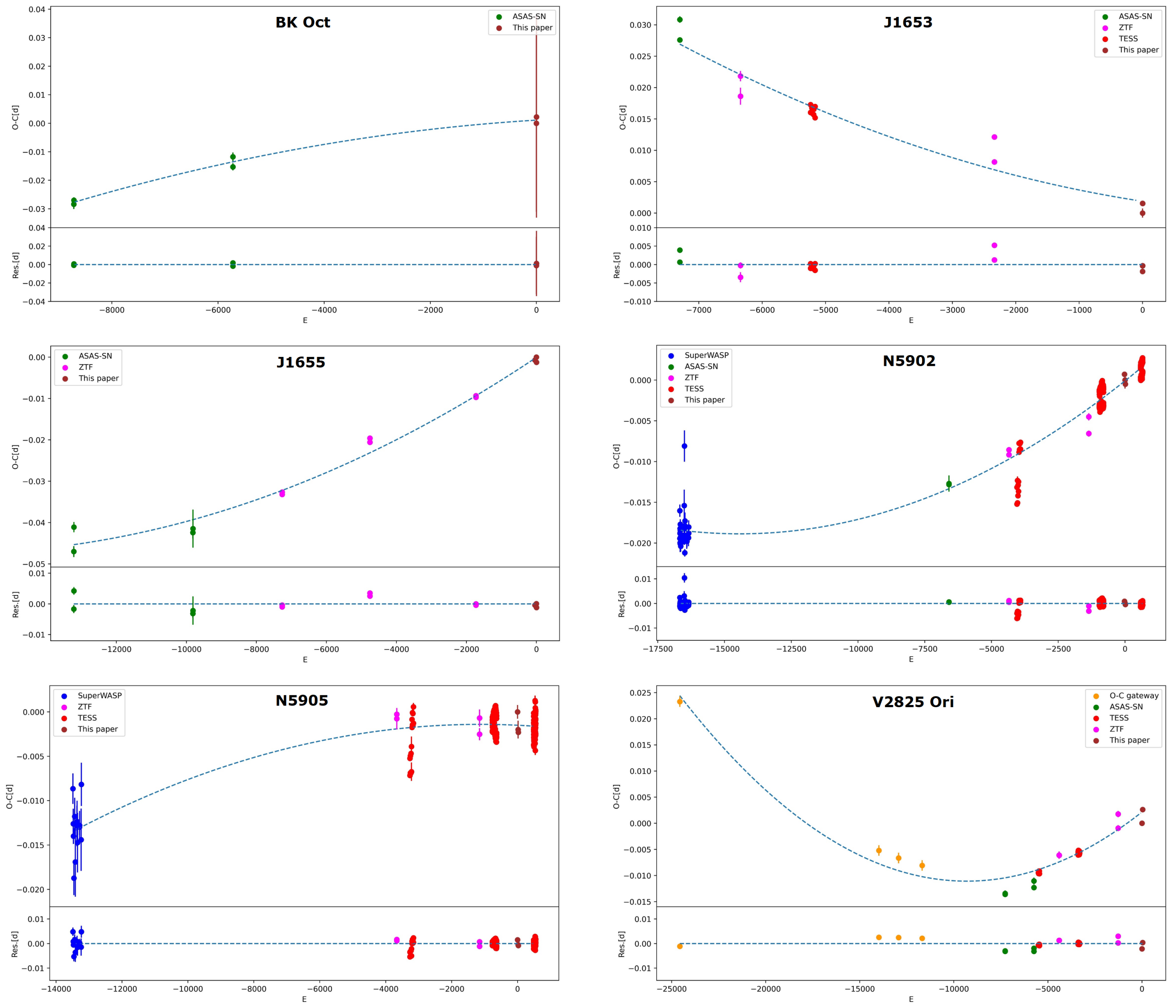

Figure 1. The O-C diagrams of the seven binary systems.

Then, we attempted to determine an acceptable theoretical fit on the observational data using the initial values. In addition, we used PHOEBE's optimization tool to improve light curve solution output and provide the desired outcomes for the next phase.

The MCMC approach based on the emcee package (Foreman-Mackey et al. 2013) was used to determine the final values of the parameters and their uncertainty. Mass ratio q, inclination i, fillout factor f, and effective stars' temperatures $T_{1,2}$ were the five main parameters considered for the MCMC modeling process. We selected the Gaussian distribution that adequately encompasses the entire observational light curve and employed 28 walkers, 3000 iterations, and a 500 burn-in in the MCMC sampling. The light curve analysis indicated no target system displayed a third body l_3.

Table 8 presents the outcomes of the light curve solutions. The corner plot of one target system is displayed as an example in Figure 3, and the corner plots for the other systems are available in the online version of this study. Figure 4 displays the binary systems' observed and final synthetic light curves. The binary systems' three-dimensional (3D) views are displayed in Figure 5.

6 ABSOLUTE PARAMETERS ESTIMATIONS

There are various methods to estimate the absolute parameters of the contact binary systems. When just photometric data is available, one method for this estimation is the Gaia DR3 parallax, which was explained in the Poro et al. (2024a) study. The accuracy of estimation of absolute parameters using Gaia DR3 parallax depends on the input parameters; however, with A_V higher than 0.4 mag., this method's results could be unreliable. Using the 3D dust map based on the Gaia DR3 distance, we computed A_V (Green et al. 2019). G5842, N5902, N5905, and V2825 Ori show inappropriate values of A_V to use Gaia DR3 parallax to estimate absolute parameters (Table 9). Therefore, we used an empirical parameter relationship between the orbital period and the semi-major axis ($P - a$) to estimate the

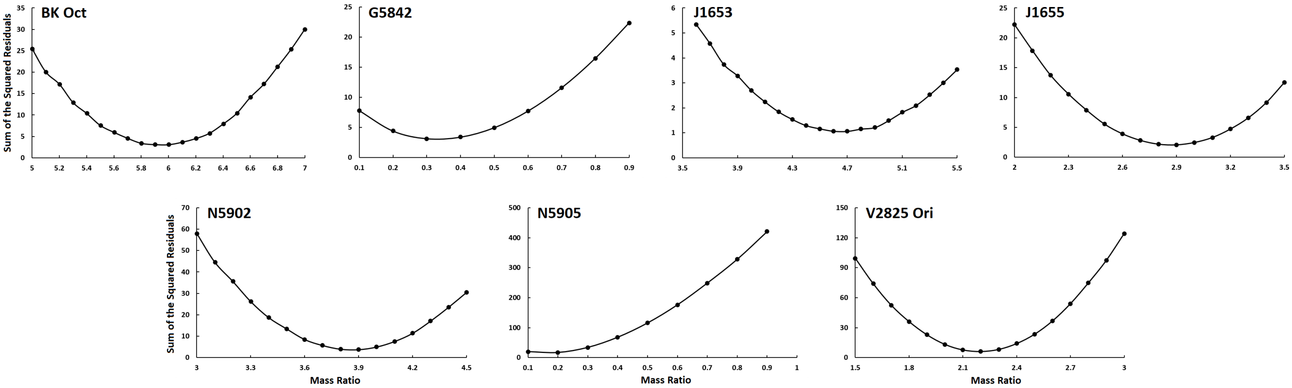

Figure 2. Sum of the squared residuals as a function of the mass ratio.

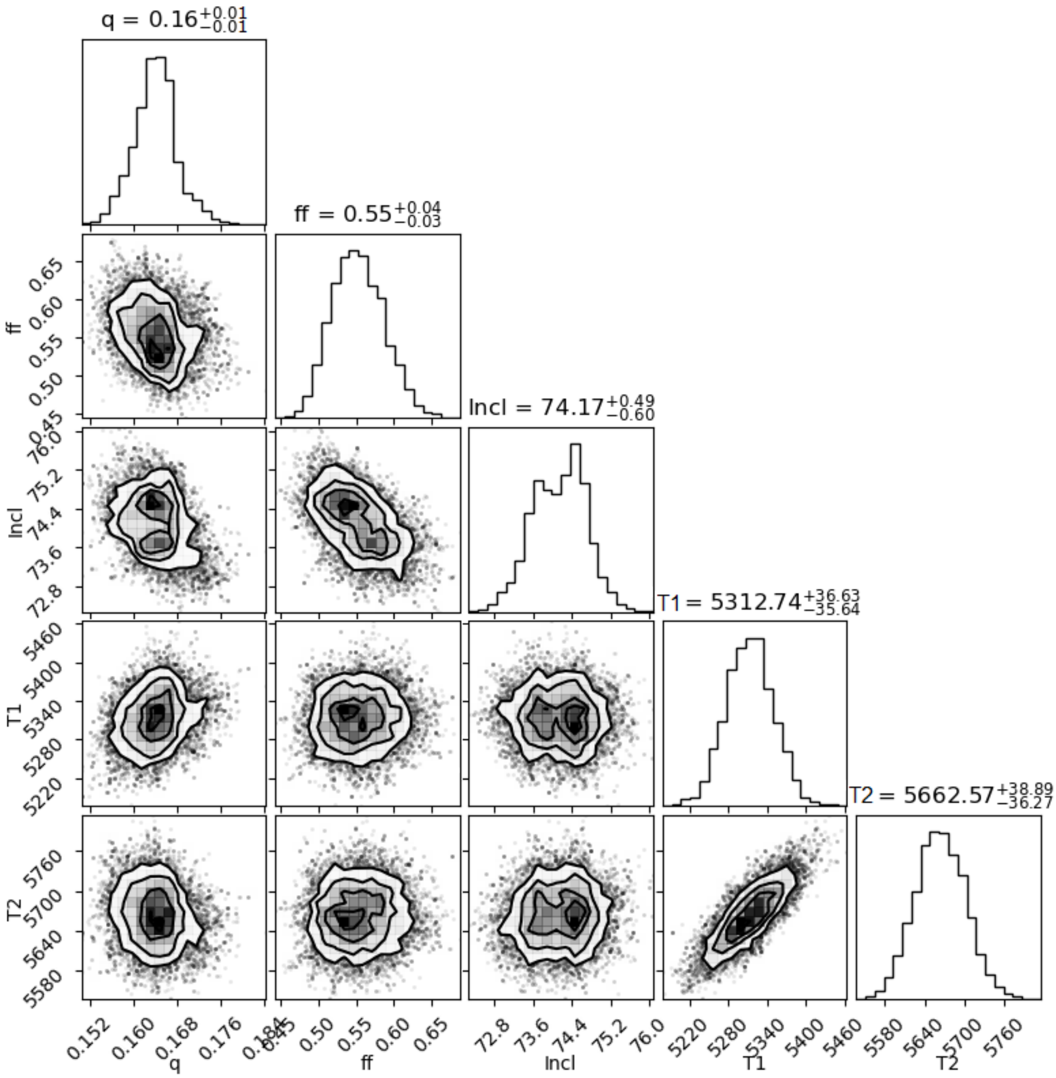

Figure 3. The corner plots of the N5905 system were determined by MCMC modeling.

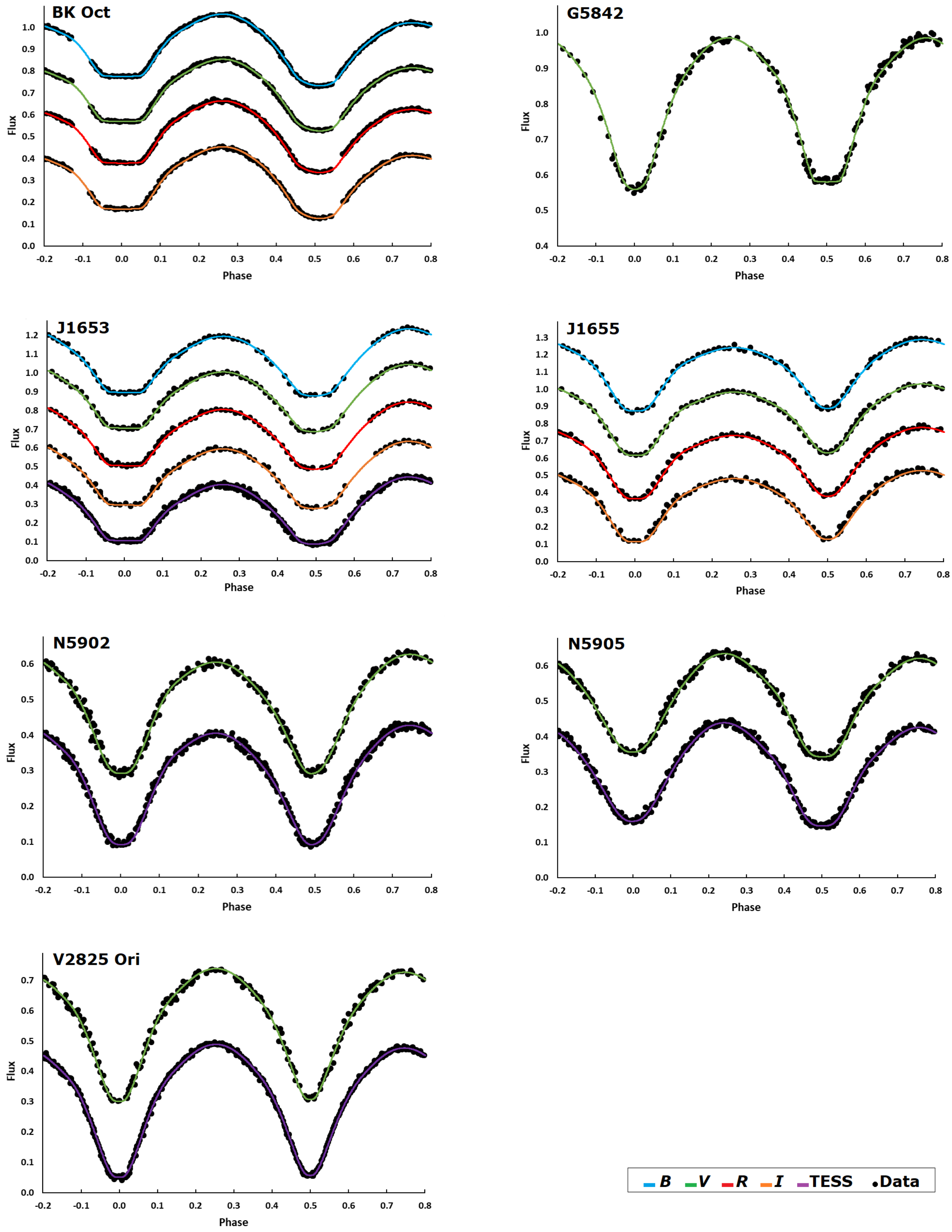

Figure 4. The black dots show the observed light curves of the systems, and the synthetic light curves were generated using the light curve solutions. Each filter is marked with color.

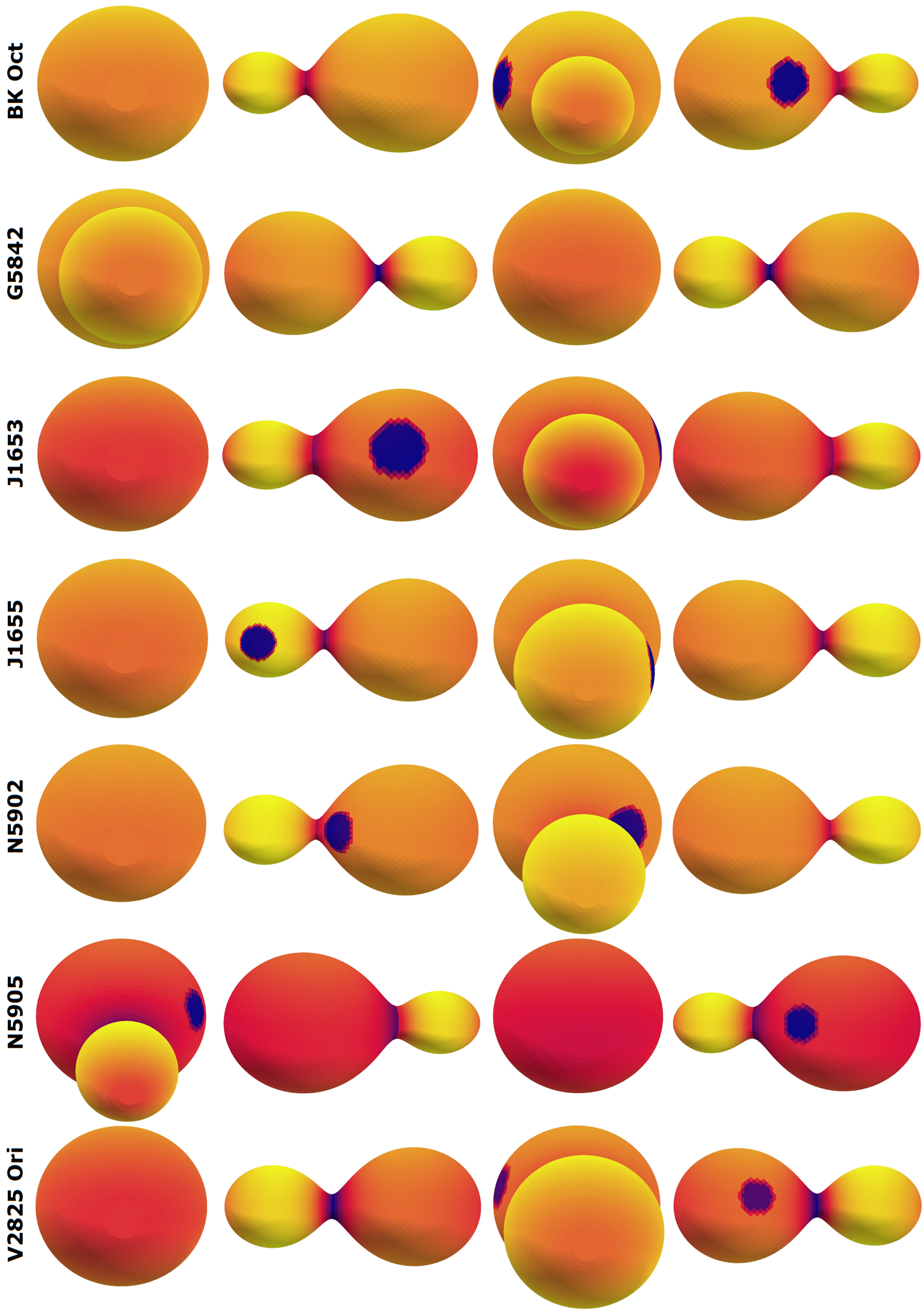

Figure 5. 3D view of stars in the target binary systems.

Table 8. Light curve solutions of the target binary stars.

Parameter	BK Oct	G5842	J1653	J1655	N5902	N5905	V2825 Ori
T_1 (K)	$5724^{+(17)}_{-(15)}$	$4756^{+(33)}_{-(38)}$	$5038^{+(71)}_{-(71)}$	$4816^{+(80)}_{-(72)}$	$5858^{+(39)}_{-(39)}$	$5313^{+(37)}_{-(36)}$	$5918^{+(74)}_{-(75)}$
T_2 (K)	$5646^{+(17)}_{-(13)}$	$4831^{+(37)}_{-(40)}$	$4904^{+(73)}_{-(70)}$	$4676^{+(72)}_{-(68)}$	$5568^{+(39)}_{-(35)}$	$5663^{+(39)}_{-(36)}$	$5744^{+(70)}_{-(70)}$
$q = M_2/M_1$	$5.95^{+(3)}_{-(6)}$	$0.34^{+(1)}_{-(1)}$	$4.53^{+(9)}_{-(9)}$	$2.87^{+(8)}_{-(9)}$	$3.88^{+(8)}_{-(10)}$	$0.16^{+(1)}_{-(1)}$	$2.19^{+(4)}_{-(6)}$
i°	$85.08^{+(87)}_{-(58)}$	$88.36^{+(60)}_{-(59)}$	$85.18^{+(1.62)}_{-(1.77)}$	$81.49^{+(81)}_{-(92)}$	$76.52^{+(34)}_{-(28)}$	$74.17^{+(49)}_{-(60)}$	$83.22^{+(57)}_{-(56)}$
f	$0.29^{+(1)}_{-(2)}$	$0.08^{+(2)}_{-(2)}$	$0.64^{+(4)}_{-(4)}$	$0.11^{+(2)}_{-(4)}$	$0.15^{+(2)}_{-(2)}$	$0.55^{+(4)}_{-(3)}$	$0.16^{+(1)}_{-(1)}$
$\Omega_1 = \Omega_2$	10.15(32)	2.54(2)	8.17(23)	6.38(7)	7.66(10)	2.07(5)	5.42(10)
$l_1/l_{tot}(V)$	0.182(1)	0.707(4)	0.238(1)	0.319(1)	0.261(1)	0.792(3)	0.354(1)
$l_2/l_{tot}(V)$	0.818(5)	0.293(1)	0.762(4)	0.681(2)	0.739(4)	0.208(1)	0.646(2)
$r_{(mean)1}$	0.252(13)	0.481(5)	0.293(24)	0.299(7)	0.277(8)	0.564(21)	0.325(12)
$r_{(mean)2}$	0.549(11)	0.295(5)	0.545(19)	0.481(19)	0.509(7)	0.261(24)	0.461(11)
$Col.^{\circ}$(spot)	95(1)		100(1)	86(1)	95(1)	77(1)	104(2)
$Long.^{\circ}$(spot)	299(3)		84(1)	263(2)	29(1)	56(1)	289(2)
$Radius^{\circ}$(spot)	15(1)		19(1)	24(2)	15(1)	12(1)	14(1)
T_{spot}/T_{star}	0.82(1)		0.87(1)	0.80(1)	0.79(1)	0.88(1)	0.91(1)
Component	Secondary		Secondary	Primary	Secondary	Primary	Secondary

absolute parameters of the target systems (Poro et al. 2024c). The $P-a$ empirical relationship was updated by Poro et al. (2024b) utilizing 414 contact binary systems with orbital periods shorter than 0.7 days (Equation 3).

$$a = (0.372^{+0.113}_{-0.114}) + (5.914^{+0.272}_{-0.298}) \times P \tag{3}$$

The estimation process for the absolute parameters started with calculation $a(R_{\odot})$ using P(day). We used the average uncertainty in Equation 3. Then, Kepler's famous third law equation and the mass ratio (q) from the light curve solutions were used to determine each star's mass and uncertainty (Equations 4 and 5).

$$M_1 = \frac{4\pi^2 a^3}{GP^2(1+q)} \tag{4}$$

$$M_2 = q \times M_1 \tag{5}$$

The radius (R) of each star was calculated using $r_{mean1,2}$ from the light curve solutions and equation 6,

$$R = a \times r \tag{6}$$

It is possible to estimate the luminosity of the components by having each star's radius and effective temperature using an astrophysics equation for stars (Equation 7),

$$L = 4\pi R^2 \sigma T^4 \tag{7}$$

The absolute bolometric magnitude (M_{bol}) was calculated using the estimated luminosity and the relationship between the star parameters (Equation 8). We set the Sun's absolute bolometric magnitude to be 4.73^{mag} based on the Torres (2010) study.

$$M_{bol1,)} = M_{bol\odot} - 2.5 \times log\left(\frac{L_{1,2}}{L_{\odot}}\right) \tag{8}$$

We estimated the surface gravity (g) of the stars on a logarithmic scale using the mass and radius parameters of stars (Equation 9).

$$g = G_{\odot}(M/R^2) \tag{9}$$

The orbital angular momentum (J_0) of each system was estimated using the Eker et al. (2006) study (Equation 10),

$$J_0 = \frac{q}{(1+q)^2}\sqrt[3]{\frac{G^2}{2\pi}M^5 P} \tag{10}$$

where q is the mass ratio, M is the total mass of the system, P is the orbital period, and G is the gravitational constant.

The results of estimating seven binary systems' absolute parameters are presented in Table 9.

7 DISCUSSION AND CONCLUSION

We conducted the first in-depth photometric study on seven total eclipse contact binary stars, including orbital period variations, light curve solutions, and absolute parameter estimations. These target systems were observed at four northern and southern hemisphere

Table 9. Estimated absolute parameters of the systems.

Parameter	BK Oct	G5842	J1653	J1655	N5902	N5905	V2825 Ori
$M_1(M_\odot)$	0.24(7)	1.04(33)	0.26(8)	0.36(12)	0.33(9)	1.56(41)	0.50(14)
$M_2(M_\odot)$	1.41(39)	0.36(12)	1.17(37)	1.04(34)	1.27(37)	0.25(7)	1.09(32)
$R_1(R_\odot)$	0.64(9)	0.94(10)	0.60(11)	0.59(7)	0.68(8)	1.65(20)	0.79(10)
$R_2(R_\odot)$	1.40(15)	0.58(7)	1.11(15)	0.95(13)	1.25(13)	0.77(14)	1.12(13)
$L_1(L_\odot)$	0.40(13)	0.41(11)	0.21(10)	0.17(6)	0.49(14)	1.97(57)	0.68(23)
$L_2(L_\odot)$	1.80(43)	0.16(5)	0.64(23)	0.39(15)	1.35(33)	0.54(23)	1.22(37)
$M_{bol1}(mag.)$	5.72(30)	5.71(26)	6.44(43)	6.67(32)	5.51(27)	4.00(28)	5.14(32)
$M_{bol2}(mag.)$	4.09(23)	6.70(27)	5.21(34)	5.76(35)	4.41(24)	5.39(39)	4.51(29)
$log(g)_1(cgs)$	4.19(1)	4.51(3)	4.30(3)	4.46(2)	4.29(1)	4.19(1)	4.34(1)
$log(g)_2(cgs)$	4.29(2)	4.47(3)	4.42(1)	4.50(1)	4.35(3)	4.07(4)	4.38(2)
$a(R_\odot)$	2.55(22)	1.95(19)	2.03(19)	1.97(19)	2.45(21)	2.93(24)	2.42(21)
$J_0(cgs)$	51.40(18)	51.42(20)	51.34(20)	51.43(20)	51.49(18)	51.48(17)	51.61(18)
$A_V(mag.)$	0.173(1)	0.896(16)	0.191(1)	0.105(1)	0.401(16)	0.858(5)	0.501(3)

observatories. Based on the results, the following are presented as discussions and conclusions:

A) Based on the O-C diagram analysis, we obtained that the orbital periods of four targets show a long-term increase and two targets show a long-term orbital period decrease. We assumed that the orbital period variations are caused by conservative material transfer. Equation 11 (Kwee 1958),

$$\frac{\dot{P}}{P} = -3\dot{M}(\frac{1}{M_1} - \frac{1}{M_2}), \tag{11}$$

was used to calculate material transfer rates, and the results are shown in Table 7. Because the time span of the O-C diagram for all targets is very short, more observations are needed to confirm the present results in the future.

B) Light curve analysis was carried out with the PHOEBE Python code, and MCMC. The light curve solutions of the six target systems required the addition of a cold or hot starspot due to the asymmetry in the maxima. The starspot is related to the O'Connell effect, which is an observational phenomenon that mostly occurs in contact binary systems (O'Connell 1951b). According to the results, the target systems' stars have temperatures ranging from 4676 K to 5918 K. It was found that the G5842 (75 K) and N5905 (350 K) systems have the minimum and maximum temperature differences (ΔT) between the two companion stars, respectively (Table 10). We identified the spectral category of the stars of the systems in Table 10 based on the studies of Cox (2000) and Eker et al. (2018). The temperature difference between two stars in contact binary systems is roughly five percent, which is true for our target systems.

C) We used the empirical relationship $P-a$ to estimate the absolute parameters of the systems. So, each star's mass and the system's total mass (M_{tot}) were calculated. The orbital angular momentum of each system was estimated using the orbital period, total mass of the system, and parameters of the mass ratio of our findings and Equation 10 from the Eker et al. (2006) study. We show the location of each system in the J_0-M_{tot} diagram (Figure 6) based on the results in Table 9. The area below the quadratic line in Figure 6 is associated with contact binary stars, whereas the area above represents detached systems. Consequently, seven target systems are below the quadratic fit and in the contact binary region.

D) We found that the target systems are eclipsing contact binary

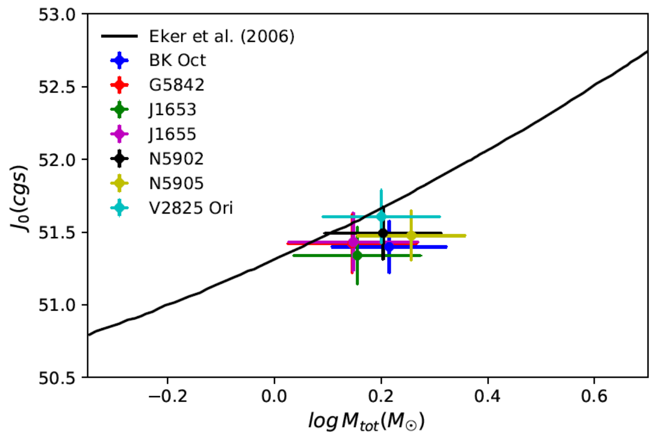

Figure 6. Location of the seven systems on the $log(J_0) - log(M_{tot})$ diagram. Detached binaries are above the quadratic borderline and contact systems are below it.

systems based on their light curve solution results such as mass ratios, fillout factors, and orbital inclinations. Therefore, the subtype of each system is possible to identify based on the effective temperature and mass of the stars. W UMa contact binary stars are divided into A and W subtypes (Binnendijk 1970). So, if the less massive component has a higher effective temperature, the system is classified as a W subtype, and if the more massive component is a hotter star, it is classified as an A subtype. According to the definition, the seven studied systems are of the W subtype (Table 10).

E) We displayed the evolution state of the systems on the Mass-Radius ($M-R$) and Mass-Luminosity ($M-L$) diagrams (Figure 7) based on the estimation of absolute parameters. The figures showed the star positions relative to the Terminal-Age Main Sequence (TAMS) and Zero-Age Main Sequence (ZAMS) lines from the Girardi et al. (2000) study. According to the light curve analysis and estimation of absolute parameters, stars with lower mass and radius in target systems have a higher temperature. Since the stars' luminosity is more dependent on their radius (Equation 7), our target has a smaller luminosity. Therefore, as shown in Figure 7, the lower mass components are located in the region above the TAMS. Also, the stars with more mass are around ZAMS.

F) Many studies have been done on low mass ratio contact binary systems ($q \leqslant 0.25$), and there are still many questions (Li et al. 2022, Li et al. 2024a). The investigations of contact binaries with low mass ratios are crucial to understanding the merging process and low-mass ratio limit. BK Oct and N5905, with respective mass ratios of $1/q = 0.17$ and $q = 0.16$, are on the border of systems with extremely low mass ratios (Li et al. 2024a, Table 10).

Examining the dynamic stability of contact binaries requires knowing the ratio of the spin angular momentum (J_{spin}) to the orbital angular momentum (Hut 1980). Therefore, we used the following equation from the Yang & Qian (2015) study to determine the J_{spin}/J_0 for two target systems.

$$\frac{J_{spin}}{J_0} = \frac{1+q}{q}[(k_1 r_1)^2 + (k_2 r_2)^2 q] \tag{12}$$

In Equation 12, q is mass ratio, $k_{1,2}$ is the dimensionless gyration radius, and $r_{1,2}$ is the relative radius. We have adopted the values of $k_{1,2}$ from Li & Zhang (2006). We found that the values of J_{spin}/J_0 for BK Oct= 0.053 and N5905= 0.049 and the perspective of the J_{spin}/J_0 for these two systems are dynamically stable (Li & Zhang 2006). According to the Wadhwa et al. (2021) study, computation indicates that they must be unstable if their instability mass ratios q_{inst} are smaller than $q_{inst} = 0.055$ and $q_{inst} = 0.045$, for BK Oct and N5905, respectively.

G) Determining each star's initial mass is required to understand how stars in the contact binary system have evolved (Li et al. 2022). We used Yildiz & Doğan (2013) method for these calculations. So, the initial mass of companion stars was obtained using two Equations 13 and 15, respectively.

$$M_{2i} = M_2 + \Delta M = M_2 + 2.50(M_L - M_2 - 0.07)^{0.64} \tag{13}$$

$$M_L = (\frac{L_2}{1.49})^{1/4.216} \tag{14}$$

$$M_{1i} = M_1 - (\Delta M - M_{lost}) = M_1 - \Delta M(1-\gamma) \tag{15}$$

Where in Equations 13 and 15, M_1 and M_2 were the mass of the stars at present, M_{1i} and M_{2i} were the initial masses, M_L is the mass due to mass-luminosity relation (Equation 14), M_{lost} is the mass lost by the binary system, and γ is the ratio M_{lost} to ΔM. M_{1i} was computed using Yildiz & Doğan (2013)'s mean value of $\gamma = 0.664$. Also, we used the reciprocal mass ratio ($0 < 1/q < 1$) for these calculations. The calculations' outcome is listed in Table 10. We found that these results are consistent with those reported by Yildiz & Doğan (2013) and Yıldız (2014).

H) Recently, studies have been published that include automatic light curve analysis for determining some main parameters of contact systems using photometric light curves. These studies try to analyze a large number of contact systems and present parameters $T_{1,2}$, q, i, and f as an outcome, which is an important goal. However, the accuracy of the results of these studies is associated with doubts that have not been addressed.

The Li et al. (2024b) study presented the distributions of parameters of 11,111 short-period contact binary systems. This investigation included four of our target systems: J1653, N5902, N5905, and V2825 Ori. They used MCMC and neural networks to obtain the systems' mass ratio, orbital inclination, fillout factor, and temperature ratio. The accuracy of observational data is the most important factor in photometric analysis. The Li et al. (2024b) study used ASAS-SN V-band light curves. The majority of ASAS-SN data have scattered in the light curve; they utilized the Laflfler-Kinman string length (LKSL) to select light curves. LKSL is a statistical measure that is used to quantify the degree of scatter in the light curve data. A lower LKSL value indicates a more regular and consistent light curve (less scatter), while a higher LKSL value suggests greater variability and irregularity in brightness. The usage of LKSL cannot generally result in the selection of suitable light curves because it examines the entire light curve, and while there is little scatter in some parts of the light curve, a lot of scatter may be observed at the minima or maxima. For this reason, there is a large uncertainty in the orbital inclination in the results of Li et al. (2024b). Therefore, it is necessary to use data from other databases (e.g., TESS, Gaia) in addition to the ASAS-SN so that the amount of dispersion does not affect the results of light curve solutions.

Based on the Poro et al. (2024a) study, the difference between the calculated temperature in the light curve solution and the reported temperature of Gaia DR3 is important in evaluating the accuracy of the light curve analysis and absolute parameter outcomes. Li et al. (2024b) have used the period-temperature relationship to calculate the effective temperature of the stars. According to their results, the difference between the hotter component and the reported temperature of Gaia DR3 was J1653=770 K, N5902=286 K, N5905=334 K, and V2825 Ori=237 K. It is necessary to measure the range of temperature difference resulting from light curve analysis and Gaia DR3 to find out if this difference is acceptable for the four target systems or not. We used a sample of 102 contact systems with spectroscopic and photometric analysis and estimated the initial temperature with various methods (Table 11). The hotter stars from the selected systems and the reported temperatures of Gaia DR3 are also listed in Table 11. As shown in Figure 8 and based on a linear fit to the data (Equation 16), the uncertainty is less than ≈ 400 K.

$$T_h = (0.88 \pm 0.06) \times T_{Gaia} + (925.12 \pm 363.67) \tag{16}$$

Therefore, the Li et al. (2024b) study for the J1653 system reports a large temperature and unacceptable difference with Gaia DR3. The difference between the temperature reported by Gaia DR3 (Table 10) and the light curve analysis results in this study (Table 8) for seven target systems is lower ≈ 400 K.

DATA AVAILABILITY

Ground-based data are available in the paper's online supplement. We also used TESS photometric data in this study, which is available on the MAST portal.

ACKNOWLEDGMENTS

This manuscript was prepared by the BSN project organization. Work by Kai Li was supported by the National Natural Science Foundation of China (NSFC) (No. 12273018) and by the Qilu Young Researcher Project of Shandong University. Ground-based observations of two systems (J1653 and J1655) were conducted with the cooperation of the Observatorio Astronómico Nacional on the Sierra San Pedro Mártir (OAN-SPM), Baja California, México. We used IRAF, distributed by the National Optical Observatories and operated by the Association of Universities for Research in Astronomy, Inc., under

Table 10. Some conclusions regarding the target systems.

Systems	$\Delta T_{1,2}$ (K)	Sp. category	$1/q$	Subtype	T_{Gaia} (K)	M_{1i} ($M_\odot$)	M_{2i} ($M_\odot$)	M_{lost} ($M_\odot$)
BK Oct	78	G5-G7	0.17(1)	W	5722	0.93	1.68	0.96
G5842	75	K3-K2	0.34(1)	W	4869	0.78	1.13	0.51
J1653	134	K1-K2	0.22(1)	W	5111	0.78	1.41	0.77
J1655	140	K2-K3	0.35(1)	W	4817	0.77	1.16	0.53
N5902	290	G3-G8	0.26(1)	W	5722	0.83	1.65	0.88
N5905	350	K0-G7	0.16(1)	W	5562	1.04	1.78	1.02
V2825 Ori	174	G2-G5	0.46(1)	W	5920	0.74	1.56	0.70

Table 11. The sample used to show the temperature uncertainty of the system's hotter star from the literature with the reported temperature of Gaia DR3 for them.

System	T_h	T_{Gaia}	Ref.	System	T_h	T_{Gaia}	Ref.	System	T_h	T_{Gaia}	Ref.
V757 Cen	6000	5771	1	TYC 2675-663-1	5534	5688	28	BX Dra	6980	7613	45
BW Dra	6164	5587	2	AC Boo	6250	5882	29	GSC 01511-00479	4500	4645	46
YY Eri	5600	5240	3	FG Hya	6519	5752	30	NSVS 13392702	4500	4901	46
HV UMa	7910	7089	4	RT LMi	6350	6103	30	AK Her	6500	6217	47
U Peg	5800	5928	5	QX And	6440	6145	31	HI Dra	7000	7300	47
V899 Her	5700	6442	6	V1167 Her	4900	4829	31	V2612 Oph	6280	5771	47
FN Cam	6848	6650	7	TZ Boo	5890	5789	32	AB And	5450	5349	48
AP Leo	6250	6202	8	AQ Psc	6250	6286	33	V1191 Cyg	6378	5862	49
RZ Tau	7300	6614	9	BV Eri	6881	6571	33	HI Pup	6500	5860	50
AO Cam	5900	5346	10	CK Boo	6250	6036	33	V1003 Her	6936	7258	51
SX Crv	6340	5970	11	DY Cet	6650	6313	33	LO And	6690	5874	52
V402 Aur	6775	6830	11	EE Cet	6250	6026	33	HH UMa	6550	5979	53
EL Aqr	6909	6771	12	NN Vir	7201	6922	33	V546 And	6517	5658	54
EZ Hya	6100	5608	13	OU Ser	5940	5640	33	HH Boo	5680	5571	55
AH Aur	6418	5981	14	TX Cnc	6250	5784	33	V921 Her	7700	7327	56
GM Dra	6450	6193	14	UX Eri	6093	5637	33	V781 Tau	6000	5640	57
GR Vir	6554	5700	14	V2357 Oph	5560	5684	33	V776 Cas	7000	6461	58
UV Lyn	6000	5830	15	V2377 Oph	5940	5665	33	AM Leo	6273	6325	59
V592 Per	6020	6769	15	V417 Aql	6381	5934	33	AW UMa	7410	6556	60
TV Mus	5980	5832	16	VY Sex	5960	5891	33	GW Cnc	5790	5785	61
HX UMa	6650	6100	17	XX Sex	6881	6529	33	V728 Her	6743	6728	62
V351 Peg	7580	7029	18	FT UMa	7178	6773	34	KIC 10618253	6118	6263	63
eps CrA	6678	6880	19	V1123 Tau	5920	5788	35	V502 Oph	6140	5872	64
RR Cen	6912	6903	19	V357 Peg	7000	6672	35	AD Phe	6155	6160	65
ET Leo	5500	5790	20	BO CVn	7191	7651	36	KIC 9832227	5920	5865	66
FP Boo	6980	6758	20	FU Dra	6100	5886	37	BN Ari	5278	5498	67
DX Tuc	6250	6250	21	V524 Mon	5560	5345	38	TY Pup	6915	6917	68
V870 Ara	6210	5772	21	EF Dra	6250	5736	39	V566 Oph	6456	6658	69
HN UMa	6252	6080	22	PY Vir	4830	4995	40	V972 Her	6522	6442	69
DN Boo	6095	6442	23	DU Boo	7850	7409	41	GSC 03334-00553	6514	5997	70
V345 Gem	6365	6630	24	VW LMi	6440	6533	41	NSVS 4161544	6016	5867	70
SS Ari	5860	5682	25	DZ Psc	6210	6244	42	RZ Com	5420	6045	71
V842 Her	6020	5795	26	FI Boo	5746	5726	43	CN And	6350	6288	72
CN Hyi	6500	6375	27	HV Aqr	6669	5792	44	BB Peg	6355	5525	73

(1) Maceroni et al. (1984), (2) Kaluzny & Rucinski (1986), (3) Yang & Liu (1999), (4) Csák et al. (2000), (5) Djurašević et al. (2001), (6) Özdemir et al. (2002), (7) Pribulla et al. (2002), (8) Kreiner et al. (2003), (9) Yang & Liu (2003), (10) Baran et al. (2004), (11) Zola et al. (2004), (12) Wadhwa & Zealey (2004), (13) Yang et al. (2004), (14) Gazeas et al. (2005), (15) Zola et al. (2005), (16) Qian et al. (2005), (17) Selam et al. (2005), (18) Albayrak et al. (2005), (19) Yang et al. (2005), (20) Gazeas et al. (2006), (21) Szalai et al. (2007), (22) Oh et al. (2007), (23) Şenavcı et al. (2008), (24) Yang et al. (2009), (25) Liu et al. (2009), (26) Erdem & Özkardeş (2009), (27) Özkardeş et al. (2009), (28) Caballero-García et al. (2010), (29) Nelson (2010), (30) Zola et al. (2010), (31) Djurašević et al. (2011), (32) Christopoulou et al. (2011), (33) Deb & Singh (2011), (34) Yuan (2011), (35) Ekmekçi et al. (2012), (36) Zola et al. (2012), (37) Liu et al. (2012), (38) He et al. (2012), (39) Yang (2012), (40) Zhu et al. (2013), (41) Djurašević et al. (2013), (42) Yang et al. (2013), (43) Christopoulou & Papageorgiou (2013), (44) Li & Qian (2013), (45) Park et al. (2013), (46) Lohr et al. (2014), (47) Çalışkan et al. (2014), (48) Li et al. (2014), (49) Ostadnezhad et al. (2014), (50) Ulaş & Ulusoy (2014), (51) Papageorgiou et al. (2015), (52) Nelson & Robb (2015), (53) Yılmaz et al. (2015), (54) Gürol et al. (2015a), (55) Gürol et al. (2015b), (56) Zhou et al. (2016b), (57) Li et al. (2016), (58) Zhou et al. (2016a), (59) Gorda (2016), (60) Eaton (2016), (61) Gürol et al. (2016), (62) Erkan & Ulaş (2016), (63) Şenavcı et al. (2016), (64) Xiao et al. (2016), (65) Pi et al. (2017), (66) Molnar et al. (2017), (67) Alton et al. (2018), (68) Sarotsakulchai et al. (2018), (69) Selam et al. (2018), (70) Kjurkchieva et al. (2019), (71) Nelson & Alton (2019), (72) Yildirim et al. (2019), (73) Kamalifar et al. (2020)

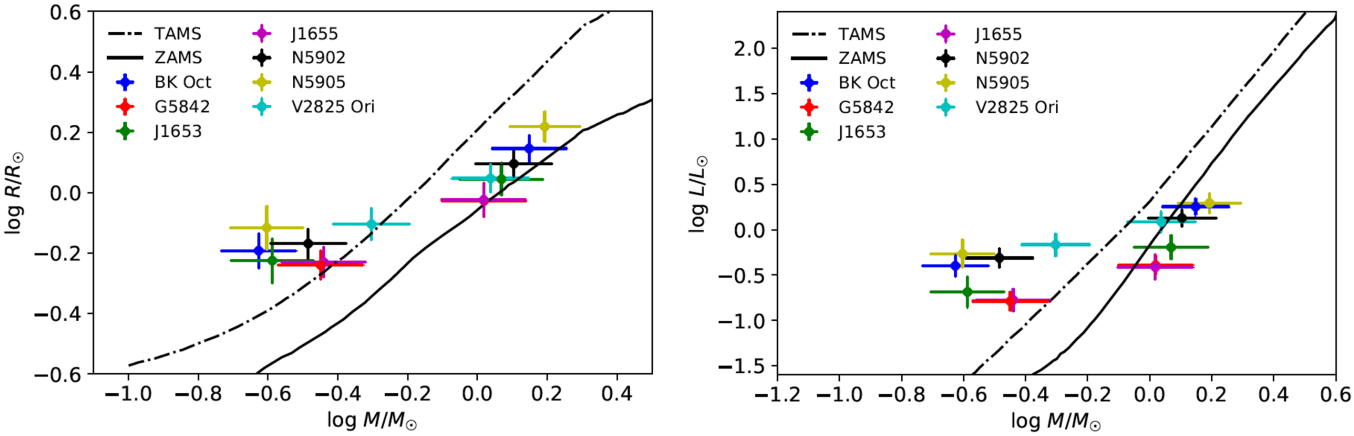

Figure 7. Position of both components on the $M - R$ and $M - L$ diagrams.

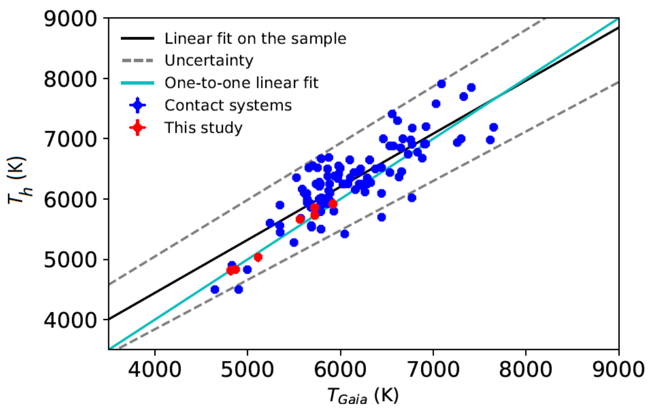

Figure 8. Hotter system star from the literature, versus the temperature reported in Gaia DR3. The red dots are the results of this study.

a cooperative agreement with the National Science Foundation. We used data from the European Space Agency mission Gaia[7]. This work includes data from the TESS mission observations. The NASA Explorer Program provides funding for the TESS mission.

ORCID IDS

Atila Poro: 0000-0002-0196-9732
Kai Li: 0000-0003-3590-335X
Ehsan Paki: 0000-0001-9746-2284
Sabrina Baudart: 0009-0004-8426-4114
Raul Michel: 0000-0003-1263-808X
Eduardo Fernández Lajús: 0000-0002-9262-4456
Fahri Alicavus: 0000-0002-1972-8400
Sacha Foschino: 0000-0003-2455-2355
Hector Aceves: 0000-0002-7348-8815
Francisco Javier Tamayo: 0000-0002-9761-9509

[7] http://www.cosmos.esa.int/gaia

REFERENCES

Akerlof C., et al., 2000, AJ, 119, 1901
Albayrak B., Djurašević G., Selam S. O., Atanacković-Vukmanović O., Yılmaz M., 2005, New Astron., 10, 163
Alton K. B., Nelson R. H., Boyd D. R. S., 2018, Acta Astron., 68, 159
Avvakumova E. A., Malkov O. Y., Kniazev A. Y., 2013, Astronomische Nachrichten, 334, 860
Baran A., Zola S., Rucinski S. M., Kreiner J. M., Siwak M., Drozdz M., 2004, Acta Astron., 54, 195
Bellm E. C., et al., 2019, PASP, 131, 068003
Binnendijk L., 1970, vistas in Astronomy, 12, 217
Bradstreet D., Guinan E., Shafter A., 1994, ASP Conf. Ser., 56, Interacting Binary Stars
Butters O. W., et al., 2010, A&A, 520, L10
Caballero-García M. D., Torres G., Ribas I., Rísquez D., Montesinos B., Mas-Hesse J. M., Domingo A., 2010, A&A, 514, A36
Castelli F., Kurucz R., 2004, AAP, 419, 725
Chen X., Wang S., Deng L., de Grijs R., Yang M., Tian H., 2020, ApJS, 249, 18
Christopoulou P. E., Papageorgiou A., 2013, AJ, 146, 157
Christopoulou P. E., Parageorgiou A., Chrysopoulos I., 2011, AJ, 142, 99
Conroy K. E., Kochoska A., Hey D., et al. 2020, APJS, 250, 34
Cox A. N., 2000, Allen's astrophysical quantities. AN Cox ed
Csák B., Kiss L. L., Vinkó J., Alfaro E. J., 2000, A&A, 356, 603
Deb S., Singh H. P., 2011, MNRAS, 412, 1787
Diethelm R., 2011, Information Bulletin on Variable Stars, 5960, 1
Djurašević G., Rovithis-Livaniou H., Rovithis P., Erkapić S., Milovanović N., 2001, A&A, 367, 840
Djurašević G., Yılmaz M., Baştürk Ö., Kılıçoğlu T., Latković O., Çalışkan Ş., 2011, A&A, 525, A66
Djurašević G., et al., 2013, AJ, 145, 80
Drake A. J., et al., 2014, ApJS, 213, 9
Eaton J. A., 2016, MNRAS, 457, 836
Eggleton P. P., 2012, Journal of Astronomy and Space Sciences, 29, 145
Eggleton P. P., Kiseleva-Eggleton L., 2002, ApJ, 575, 461
Eker Z., Demircan O., Bilir S., Karataş Y., 2006, MNRAS, 373, 1483
Eker Z., et al., 2018, MNRAS, 479, 5491
Ekmekçi F., et al., 2012, New Astron., 17, 603
Erdem A., Özkardeş B., 2009, New Astron., 14, 321
Erkan N., Ulaş B., 2016, New Astron., 46, 73
Foreman-Mackey D., Hogg D. W., Lang D., Goodman J., 2013, PASP, 125, 306
Gazeas K. D., et al., 2005, Acta Astron., 55, 123
Gazeas K. D., Niarchos P. G., Zola S., Kreiner J. M., Rucinski S. M., 2006, Acta Astron., 56, 127
Girardi L., Bressan A., Bertelli G., Chiosi C., 2000, AAPs, 141, 371

Gorda S. Y., 2016, Astrophysical Bulletin, 71, 64

Green G. M., Schlafly E., Zucker C., Speagle J. S., Finkbeiner D., 2019, ApJ, 887, 93

Gürol B., Bradstreet D. H., Okan A., 2015a, New Astron., 36, 100

Gürol B., Bradstreet D. H., Demircan Y., Gürsoytrak S. H., 2015b, New Astron., 41, 26

Gürol B., Gökay G., Saral G., Gürsoytrak S. H., Cerit S., Terzioğlu Z., 2016, New Astron., 46, 31

He J.-J., Wang J.-J., Qian S.-B., 2012, PASJ, 64, 85

Hoffman D. I., Harrison T. E., McNamara B. J., 2009, AJ, 138, 466

Hoffmeister C., 1963, Veroeffentlichungen der Sternwarte Sonneberg, 6, 1

Hut P., 1980, Astronomy and Astrophysics, vol. 92, no. 1-2, Dec. 1980, p. 167-170., 92, 167

Jayasinghe T., et al., 2018, MNRAS, 477, 3145

Jenkins J. M., et al., 2016, in Chiozzi G., Guzman J. C., eds, Society of Photo-Optical Instrumentation Engineers (SPIE) Conference Series Vol. 9913, Software and Cyberinfrastructure for Astronomy IV. p. 99133E, doi:10.1117/12.2233418

Kaluzny J., Rucinski S. M., 1986, AJ, 92, 666

Kamalifar Z., Abedi A., Roobiat K. Y., 2020, New Astron., 78, 101354

Kazarovets E. V., Samus N. N., Durlevich O. V., Kireeva N. N., Pastukhova E. N., 2015, Information Bulletin on Variable Stars, 6151, 1

Kjurkchieva D., Stateva I., Popov V. A., Marchev D., 2019, AJ, 157, 73

Kreiner J. M., et al., 2003, A&A, 412, 465

Kuiper G. P., 1941, Astrophysical Journal, vol. 93, p. 133, 93, 133

Kukarkin B. V., Kholopov P. N., Perova N. B., 1970, Information Bulletin on Variable Stars, 480, 1

Kwee K. K., 1958, Bull. Astron. Inst. Netherlands, 14, 131

Kwee K. K., van Woerden H., 1956, Bull. Astron. Inst. Netherlands, 12, 327

Latković O., Čeki A., Lazarević S., 2021, ApJS, 254, 10

Li K., Qian S. B., 2013, New Astron., 21, 46

Li L., Zhang F., 2006, MNRAS, 369, 2001

Li K., Hu S. M., Jiang Y. G., Chen X., Ren D. Y., 2014, New Astron., 30, 64

Li K., Gao D. Y., Hu S. M., Guo D. F., Jiang Y. G., Chen X., 2016, Ap&SS, 361, 63

Li K., Kim C.-H., Xia Q.-Q., Michel R., Hu S.-M., Gao X., Guo D.-F., Chen X., 2020, The Astronomical Journal, 159, 189

Li K., et al., 2021, AJ, 162, 13

Li K., Gao X., Liu X.-Y., Gao X., Li L.-Z., Chen X., Sun G.-Y., 2022, AJ, 164, 202

Li K., et al., 2024a, arXiv e-prints, p. arXiv:2411.12132

Li X.-Z., Zhu Q.-F., Ding X., Xu X.-H., Zheng H., Qiu J.-S., Liu M.-C., 2024b, ApJS, 271, 32

Liu L., Qian S. B., He J. J., Zhang J., Li L. J., 2009, Ap&SS, 321, 19

Liu L., Qian S.-B., He J.-J., Liao W.-P., Zhu L.-Y., Zhao E., 2012, PASJ, 64, 48

Lohr M. E., Hodgkin S. T., Norton A. J., Kolb U. C., 2014, A&A, 563, A34

Lucy L., 1967, ZAP, 65, 89

Lucy L. B., 1968, ApJ, 151, 1123

Maceroni C., Milano L., Russo G., 1984, A&AS, 58, 405

Malkov O. Y., Oblak E., Snegireva E. A., Torra J., 2006, A&A, 446, 785

Masci F. J., et al., 2019, PASP, 131, 018003

Molnar L. A., et al., 2017, ApJ, 840, 1

Mowlavi N., et al., 2023, A&A, 674, A16

Nelson R. H., 2010, Information Bulletin on Variable Stars, 5951, 1

Nelson R. H., Alton K. B., 2019, Information Bulletin on Variable Stars, 6266, 1

Nelson R. H., Robb R. M., 2015, Information Bulletin on Variable Stars, 6134, 1

O'Connell D. J. K., 1951a, Publications of the Riverview College Observatory, 2, 85

O'Connell D., 1951b, MNRAS, 111, 642

Oh K. D., Kim C. H., Kim H. I., Lee W. B., 2007, in Kang Y. W., Lee H. W., Leung K. C., Cheng K. S., eds, Astronomical Society of the Pacific Conference Series Vol. 362, The Seventh Pacific Rim Conference on Stellar Astrophysics. p. 82

Ostadnezhad S., Delband M., Hasanzadeh A., 2014, New Astron., 31, 14

Özdemir S., Demircan O., Erdem A., Çiçek C., Bulut İ., Soydugan E., Soydugan F., 2002, A&A, 387, 240

Özkardeş B., Erdem A., Bakış V., 2009, New Astron., 14, 461

Papageorgiou A., Christopoulou P. E., Pribulla T., Vaňko M., 2015, Ap&SS, 357, 59

Park J.-H., Lee J. W., Kim S.-L., Lee C.-U., Jeon Y.-B., 2013, PASJ, 65, 1

Pi Q.-f., Zhang L.-y., Bi S.-l., Han X. L., Wang D.-m., Lu H.-p., 2017, AJ, 154, 260

Poro A., et al., 2024a, New Astron., 110, 102227

Poro A., Tanriver M., Michel R., Paki E., 2024b, PASP, 136, 024201

Poro A., et al., 2024c, AJ, 168, 272

Pribulla T., Chochol D., Vanko M., Parimucha S., 2002, Information Bulletin on Variable Stars, 5258, 1

Prša A., Conroy K. E., Horvat M., et al. 2016, APJS, 227, 29

Qian S., 2003, MNRAS, 342, 1260

Qian S. B., Yang Y. G., Soonthornthum B., Zhu L. Y., He J. J., Yuan J. Z., 2005, AJ, 130, 224

Qian S. B., et al., 2014, ApJS, 212, 4

Ricker G. R., et al., 2010, in American Astronomical Society Meeting Abstracts #215. p. 450.06

Ricker G. R., et al., 2015a, Journal of Astronomical Telescopes, Instruments, and Systems, 1, 014003

Ricker G. R., et al., 2015b, Journal of Astronomical Telescopes, Instruments, and Systems, 1, 014003

Ruciński S., 1969, ACTAA, 19, 245

Sarotsakulchai T., et al., 2018, AJ, 156, 199

Sarvari E., Fernández Lajús E., Poro A., 2024, Research in Astronomy and Astrophysics, 24, 105002

Selam S., Albayrak B., Yilmaz M., Şenavci H. V., Özavci İ., Çetintaş C., 2005, Ap&SS, 296, 305

Selam S. O., Esmer E. M., Şenavcı H. V., Bahar E., Yörükoğlu O., Yılmaz M., Baştürk Ö., 2018, Ap&SS, 363, 34

Shappee B. J., et al., 2014, ApJ, 788, 48

Sriram K., Malu S., Choi C., Rao P. V., 2017, The Astronomical Journal, 153, 231

Stassun K. G., et al., 2018, AJ, 156, 102

Stepien K., 2006, Acta Astron., 56, 347

Stepien K., 2011, Acta Astron., 61, 139

Szalai T., Kiss L. L., Mészáros S., Vinkó J., Csizmadia S., 2007, A&A, 465, 943

Terrell D., Wilson R. E., 2005, Ap&SS, 296, 221

Tody D., 1986, in Crawford D. L., ed., Society of Photo-Optical Instrumentation Engineers (SPIE) Conference Series Vol. 627, Instrumentation in astronomy VI. p. 733, doi:10.1117/12.968154

Torres G., 2010, AJ, 140, 1158

Ulaş B., Ulusoy C., 2014, New Astron., 31, 56

Wadhwa S. S., Zealey W. J., 2004, Ap&SS, 291, 21

Wadhwa S. S., De Horta A., Filipović M. D., Tothill N. F., Arbutina B., Petrović J., Djurašević G., 2021, Monthly Notices of the Royal Astronomical Society, 501, 229

Xiao Z., Shengbang Q., Binghe H., Hao L., Jia Z., 2016, PASJ, 68, 102

Yakut K., Eggleton P. P., 2005, ApJ, 629, 1055

Yang Y.-G., 2012, Research in Astronomy and Astrophysics, 12, 419

Yang Y., Liu Q., 1999, A&AS, 136, 139

Yang Y., Liu Q., 2003, AJ, 126, 1960

Yang Y.-G., Qian S.-B., 2015, AJ, 150, 69

Yang Y. G., Qian S. B., Zhu C. H., 2004, PASP, 116, 826

Yang Y.-G., Qian S.-B., Zhu L.-Y., He J.-J., Yuan J.-Z., 2005, PASJ, 57, 983

Yang Y. G., Qian S. B., Zhu L. Y., He J. J., 2009, AJ, 138, 540

Yang Y. G., Qian S. B., Zhang L. Y., Dai H. F., Soonthornthum B., 2013, AJ, 146, 35

Yildirim M. F., Aliçavuş F., Soydugan F., 2019, Research in Astronomy and Astrophysics, 19, 010

Yıldız M., 2014, MNRAS, 437, 185

Yildiz M., Doğan T., 2013, MNRAS, 430, 2029

Yılmaz M., Baştürk Ö., Özavcı İ., Şenavcı H. V., Selam S. O., 2015, New Astron., 34, 271

Yuan J.-Z., 2011, Research in Astronomy and Astrophysics, 11, 1158

Zhou X., Qian S. B., Zhang J., Jiang L. Q., Zhang B., Kreiner J., 2016a, ApJ, 817, 133
Zhou X., Qian S.-B., Zhang J., Li L.-J., Wang Q.-S., 2016b, Advances in Astronomy, 2016, 746897
Zhu L. Y., Qian S. B., Liu N. P., Liu L., Jiang L. Q., 2013, AJ, 145, 39
Zola S., et al., 2004, Acta Astron., 54, 299
Zola S., et al., 2005, Acta Astron., 55, 389
Zola S., Gazeas K., Kreiner J. M., Ogloza W., Siwak M., Koziel-Wierzbowska D., Winiarski M., 2010, MNRAS, 408, 464
Zola S., Nelson R. H., Şenavcı H. V., Szymanski T., Kuźmicz A., Winiarski M., Jableka D., 2012, New Astron., 17, 673
Çalışkan Ş., et al., 2014, AJ, 148, 126
Şenavcı H. V., Nelson R. H., Özavcı İ., Selam S. O., Albayrak B., 2008, New Astron., 13, 468
Şenavcı H. V., Doğruel M. B., Nelson R. H., Yılmaz M., Selam S. O., 2016, Publ. Astron. Soc. Australia, 33, e043

This paper has been typeset from a TEX/LATEX file prepared by the author.